

Directed Hybridization Method for Synthesis of CuO/ZnO Nanostructures and their Electrocatalytic Properties

Majid Arvand^{1*}, Talat P.-Saravani²,
Farhang Mizani³ and Akram Pourhabib⁴

¹*Electroanalytical Chemistry Laboratory, Faculty of Chemistry,
University of Guilan, Rasht, Iran*

²*Department of Chemistry, Payame Noor University, Tehran, Iran*

³*Department of Chemistry, Faculty of Science, Imam Khomeini
International University, Qazvin, Iran*

⁴*Education Organization of Guilan Province, Rasht, Iran*

*Corresponding author: arvand@guilan.ac.ir

Received 06/11/2023; accepted 15/02/2024

<https://doi.org/10.4152/pea.2025430501>

Abstract

In this study, novel CuO/ZnO was synthesized using complex-directed hybridization and subsequent calcination (HNS/MWCNT). Then, they were employed as an electrochemical sensor for SFA. The synthesized CuO/ZnO was characterized using various techniques, including TEM, SEM, FT-IR, EDX, DPV and CV. Electrochemical studies revealed that HNS from CuO/ZnO/MWCNT modified electrode exhibited high A, more reactive sites and excellent electrochemical catalytic activity towards SFA oxidation, compared to GCE. The pH, modifier amount, SR and analyte Ct effects on oxidation i_p were investigated, to optimize experimental conditions. LoD of 0.089 μM and linear calibration range from 0.1 to 1000 μM were obtained for SFA determination on HNS from CuO/ZnO/MWCNT/GCE. The modified electrode was successfully applied for SFA determination in WW, pharmaceutical and biological samples.

Keywords: complex-directed hybridization; CV; DPV; HNS; MWCNT; SFA; ZnO/CuO.

Introduction*

In recent times, mixed metal oxide NP have gained significant attention from researchers, in diverse fields like Physics, Chemistry and material science, due to their broad practical applications, such as photocatalysis, sensing, microelectronic circuit manufacture, piezoelectric devices, fuel and solar cells [1, 2]. These NP exhibit unique properties, including high activity, special electronic properties, large surface area, chemical and optical properties [3-5]. The coupling of one metal oxide Sc with another one results in an enlarged surface area that provides more reactive sites, promotes mass and electron transfer, and prevents NC photocorrosion, ultimately enhancing their efficiency.

The capability of tuning E_{gap} , by incorporating two different materials, is a significant advantage in nanotechnology field. Moreover, NC development with controllable

*The abbreviations and symbols lists are on pages 282-283.

shapes, sizes and surface properties is crucial for diverse practical applications. Among all possible p-n type mixed Sc, like TiO₂/NiO [3], CuO/SnO₂ [5], SnO₂/NiO [6, 7] and CuO/TiO₂ [8, 9], CuO/ZnO have garnered considerable attention from researchers. ZnO and CuO are n- and p-type Sc, with E_{gap} of 3.37 and 1.2 eV, respectively, and conductivities ranging from 10⁻⁷ to 10⁻³ S/cm, for ZnO, and 10⁻⁴ S/cm, for CuO [10-14].

CuO-ZnO heterojunctions have been synthesized by various researchers, such as [15-17], who have demonstrated their potential in various environmental fields. Furthermore, several techniques have been employed by researchers, to prepare NC from CuO-ZnO, including thermal decomposition [2], co-precipitation [18], chemical vapor deposition [19], sol-gel and wet-impregnation methods [20], heating brass in air [21] and complex-directed hybridization [22]. [18, 23] have observed better photocatalytic performance of NC from CuO-ZnO than their individual elements. Similarly, [24, 25] have reported better gas-sensing ability of NC from Cu-doped ZnO than pure ZnO. [26] has shown that NC from CuO-ZnO are better supercapacitors than pure CuO.

CNT possess unique properties, including high electrical conductivity, surface/volume ratio and mechanical strength, chemical stability and chemically modifiable large surface area. These properties make them fascinating materials for electroanalysis. Combining CNT with other NP, such as NC from CuO/ZnO, can improve electron transfer kinetics and electrochemical sensor sensitivity [27, 28].

SFA is a crucial type of sulfonamide, used as a synthetic antibacterial agent for treating various dermatological abnormalities [29, 30]. Several analytical methods are available for assessing sulfonamides in biofluids, WW and pharmaceutical products, including high-performance liquid (with UV), gas and micellar electrokinetic capillary chromatography, fluorescence, mass spectrometry, capillary zone electrophoresis, spectrophotometry and potentiometry [31-36]. However, these analyses are subject to complex biological matrix effects, and interference must be corrected through sample pretreatment. Electroanalytical methods are gaining interest among researchers for drugs and biomolecules determination, due to their low cost, ease of instrumentation, high sensitivity and selectivity, and the possibility of analysis without complicated sample pretreatment [31].

In this study, a GCE was modified with MWCNT and NP of CuO/ZnO derived from a complex-directed hybridization method, to develop a novel, simple and cost-effective NC. The modified electrode was used to determine SFA in various bio samples, and the results showed its high sensitivity and selectivity.

Experimental methods

Reagents and solutions

All chemical reagents employed in the experiments were analytical grade, and not further purified. Zn(CH₃COO)₂·2H₂O, Cu(NO₃)₂·3H₂O (99%), HCl, CH₃COOH, CH₃COONa, KCl, K₃[Fe(CN)₆], H₂C₂O₄·2H₂O (Merck, Darmstadt, Germany), DMF (Sigma-Aldrich) and SFA (Behdasht Kar company, Rasht, Iran) were purchased. MWCNT purity was >95% (purchased from US Research Nanomaterials Inc.). A

0.1 M ABS (pH 4.5) was prepared by mixing CH_3COOH and CH_3COONa solutions. All solutions were prepared and diluted using high-quality deionized water.

Apparatus

Electrochemical measurements were performed with an Autolab PGSTAT 30 electrochemical analyzer (Eco Chemie BV, Utrecht, the Netherlands). A conventional three-electrode cell was used, at 25 ± 1 °C. A saturated Ag/AgCl electrode, a Pt wire and a modified GCE (PTFE/Kel-F coat material, 3 mm diameter, 7.07 mm^2 geometric area, 80 mm length and 6.35 mm outer diameter) were used as reference, auxiliary and working electrodes, respectively. Amperometry analysis was performed by PalmSens analyzer, at E of 0.88 V, under continuous stirring. Pulse amplitude of 0.025 V, pulse interval time of 0.5 s and SR of 0.01 V/s were chosen as optimum instrumental parameters for DPV. All pH values were measured with a Metrohm pH meter (model 827, Herisau, Switzerland). TEM images were obtained for NC morphology characterization, using Tecnai G2 20 TEM. Chemical composition and surface morphology were determined using EDX spectra and SEM images, by LEO 1400 VP, Zeiss (Cambridge, UK). Biochrom WPA Biowave II UV-vis spectrophotometer was used to record all samples UV-vis absorption spectra, in the range from 200 to 900 nm.

Synthesis of HNS from CuO/ZnO by complex-directed hybridization

HNS from CuO/ZnO were synthesized using complex-directed hybridization and subsequent calcination method. Specifically, 25 mL (0.01 M) each of $\text{Zn}(\text{CH}_3\text{CO}_2)_2$ and $\text{Cu}(\text{NO}_3)_2$ solutions were mixed and vigorously stirred at 45 °C, for 10 min. The resulting solution was then heated under reflux, for more 50 min, at the same temperature. The resulting products were subsequently dried and annealed at 350 °C, for 3 h [22].

Preparation of modified electrode

Initially, the GCE was polished with alumina powder and subsequently cleaned in ethanol and double-distilled water, for 2 min, using ultrasonication (Sono Swiss SW3-H, 38 kHz, Switzerland), to eliminate physically adsorbed pollutants. The prepared electrode was dried at room temperature, and immediately used for modification. Subsequently, 10 mg MWCNT and 5 mg HNS from CuO/ZnO were dispersed in 1 mL DMF, using sonication, for the electrode modification. Next, 3 μL NC suspension were applied to the clean GCE surface, using a micro syringe (Hamilton 84250 Model 701N), and dried at room temperature. The casting process was repeated twice, to prepare each electrode. The resulting electrode was denoted as HNS from CuO/ZnO/MWCNT/GCE. The same process was used to prepare MWCNT/GCE, CuO/MWCNT/GCE and ZnO/MWCNT/GCE electrodes.

Samples preparation

This study examined three types of samples: SFA ophthalmic drops (10%) purchased from Sina Darou, healthy human blood serum samples collected from sundry laboratories, and industrial WW prepared from a pharmaceutical company. The collected blood serum and WW samples were stored at 4 °C, for 2 days. 1 mL SFA ophthalmic drops or blood serum and 10 mL WW were separately diluted with an ABS,

at a pH of 4.5, to reach a final volume of 25 mL. Notably, WW samples were filtered and diluted with a 0.1 M HCl solution (20:1 volume ratio), prior to investigation [37].

Results and discussion

Characterization of HNS from CuO/ZnO

Fig. 1 shows FT-IR spectra of HNS from CuO, ZnO, CuO/ZnO and CuO/ZnO MWCNT. There are four spectra in Fig. 1, with two absorptions bands around 1630-1670 and 3419-3435 cm^{-1} , which are assigned to antisymmetric stretching vibrations of H-O-H and water O-H vibrations on the NP surface, respectively.

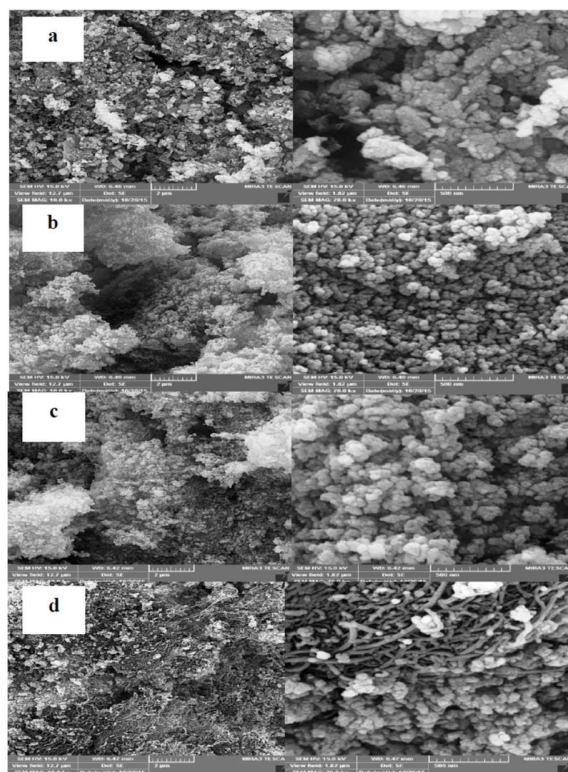


Figure 1: SEM images of -(a) CuO; (b) ZnO; (c) HNS from CuO/ZnO; and (d) HNS from CuO/ZnO/MWCNT.

Spectrum 1 represents absorptions around 521 and 1122 cm^{-1} , belonging to Cu-O and Cu-OH stretching vibrations, respectively. Absorption peaks in 436, 522 and 875 cm^{-1} regions, in spectrum 2, are related to Zn-O stretching vibrations. Fig. 1 (spectrum 3) of HNS from CuO/ZnO indicates Zn-O stretching vibrations at 454 and 812 cm^{-1} . Also, Cu-O stretching vibration band appears at 534 cm^{-1} . In the last spectrum (Fig. 1 (spectrum 4)), it can be seen that the intensity of all Cu-O and Zn-O bands decreases, due to the presence of MWCNTs in a ratio of 2:1 [38-41].

The morphologies of HNS from CuO, ZnO, CuO/ZnO and CuO/ZnO/MWCNT were examined using SEM, at scales of 2 μm and 500 nm. Fig. 1a shows that NP from CuO were aggregated into a spherical shape, with a porous surface. Fig. 1b displays spherical

and separated NP from ZnO, with higher porosity than CuO. Fig. 1c illustrates a morphologic modification and a uniform spherical shape for HNS from CuO and ZnO, with high porosity and surface area. Furthermore, Fig. 1d confirms that the addition of HNS from CuO/ZnO improved MWCNT's surface area and properties.

Fig. 2 illustrates typical TEM images of HNS from CuO/ZnO/MWCNT, at different magnifications. It is apparent that HNS from CuO/ZnO/MWCNT are composed of spherical particles with good dispersion.

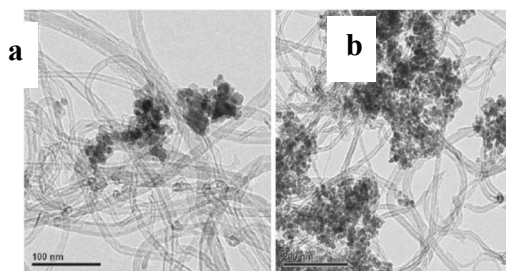


Figure 2: TEM images of HNS from CuO/ZnO with MWCNT, in the scale of -(a) 100 and (b) 200 nm.

EDX spectra were used to investigate elemental composition of HNS from CuO, ZnO, CuO/ZnO and CuO/ZnO/MWCNT. Fig. 3a shows Cu and O peaks, indicating CuO presence.

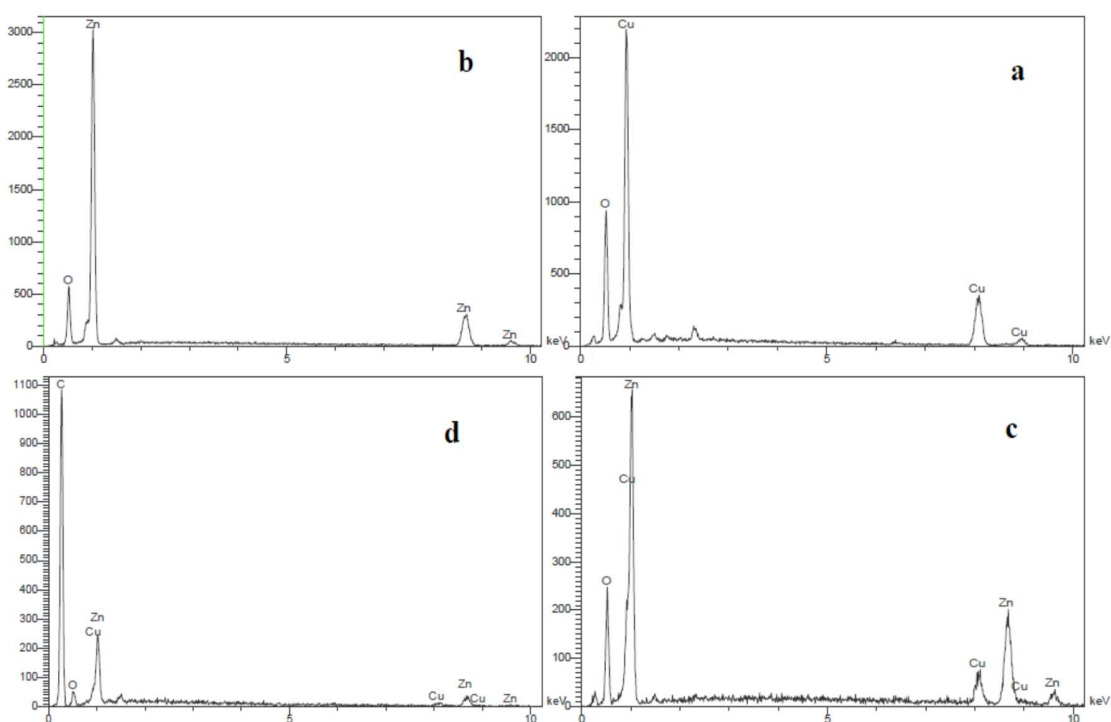


Figure 3: EDX spectra of -(a) CuO; (b) ZnO; (c) HNS from CuO/ZnO; and (d) HNS from CuO/ZnO/MWCNT.

Fig. 3b displays Zn and O peaks, which represent ZnO synthesis. Fig. 3c shows the presence of Cu, Zn and O, indicating CuO/ZnO HNS formation. Fig. 3d illustrates Cu, Zn, C and O presence, representing the formation of HNS from CuO/ZnO/MWCNT. O, Cu and Zn wt.% are reported in Table S1. According to the table, during the synthesis process, Zn:Cu ratio in HNS was 4:1.

Electrochemical performance of modified electrodes

The electrochemical behavior of an electroactive species, such as $K_3[Fe(CN)_6]/K_4[Fe(CN)_6]$ couple, is a valuable tool for evaluating the kinetic barrier of an electrode/solution interface. Therefore, voltammetric behaviors of GCE, MWCNT/GCE, CuO/MWCNT/GCE, ZnO/MWCNT/GCE and HNS from CuO/ZnO/MWCNT/GCE were studied in a 0.1 M KCl solution containing 5.0 mM $[Fe(CN)_6]^{3-/4-}$, using CV. As shown in Fig. 4, all curves exhibit a pair of $K_3[Fe(CN)_6]/K_4[Fe(CN)_6]$ reversible redox peaks.

However, compared to the GCE, MWCNT/GCE, CuO/MWCNT/GCE and ZnO/MWCNT/GCE, redox curves of HNS from CuO/ZnO/MWCNT/GCE display the highest i_p . This result indicates that the latter had faster electron transfer kinetics and a larger electroactive surface area. The A of HNS from CuO/ZnO/MWCNT/GCE was also determined by CV, in the above $K_3[Fe(CN)_6]/K_4[Fe(CN)_6]$ solution, at different SR (v) (Fig. S2), according to Randles-Sevcik equation [42]:

$$I_p = (2.69 \times 10^5)AD_0^{1/2}n^{3/2}\nu^{1/2}C_0 \quad (1)$$

where n is 1 and standard D_0 of $[Fe(CN)_6]^{3-/4-}$, at 25 °C, is 7.6×10^{-6} cm²/s [43]. The A of HNS from CuO/ZnO/MWCNT/GCE was estimated to be 0.126 cm², which is higher than A of GCE (0.024 cm²). These results indicate that the combination of HNS from CuO/ZnO with MWCNT caused the increase in the electroactive surface.

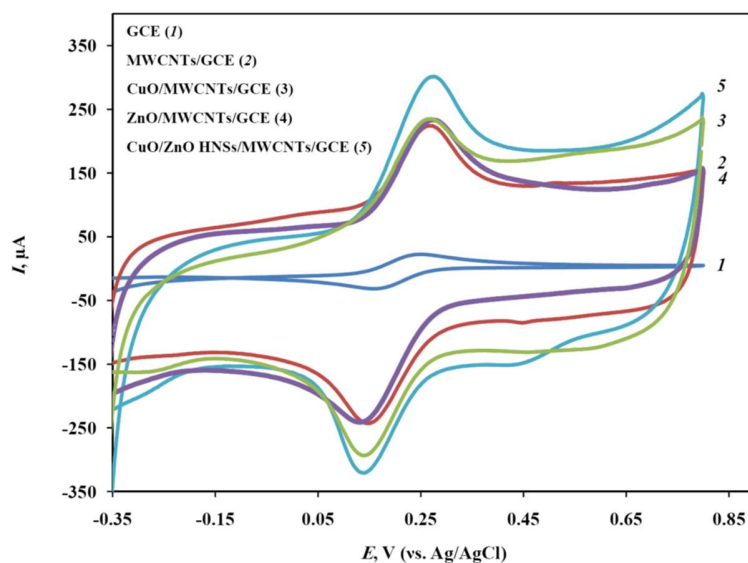


Figure 4: CV of- (1) GCE; (2) MWCNT/GCE; (3) CuO/MWCNT/GCE; (4) ZnO/MWCNT/GCE; and (5) HNS from CuO/ZnO/MWCNT/GCE, in 5 mM $K_3[Fe(CN)_6]$ with 0.1 M KCl (SR: 0.1 V/s).

Electrochemical behavior of SFA at different electrodes surfaces

In the first step, some important features of HNS from CuO/ZnO/MWCNT, such as ratios (1:1, 1:2 and 1:3) and amountd were optimized, to increase the sensitivity of HNS from CuO/ZnO/MWCNT/GCE, of which SFA's electrochemical behavior was studied using CV. Fig. 3 shows CV responses for 1×10^{-4} M SFA in a 0.1 M ABS (pH 4.5), at the SR of 0.1 V/s. It was clear that i response of HNS from CuO/ZnO/MWCNT towards SFA was weak, at (1:1). However, at 1:3, anodic i_p significantly increased. This indicates that MWCNT played an important role in the electrocatalytic performance of the modified electrode. Although the ratio of 1:3 showed higher i values, it caused more base i and instability on the GCE (Table 2). Finally, 1:2 was selected, for HNS from CuO/ZnO/MWCNT, as the optimum ratio.

Effect of solution pH

The selection of an appropriate buffer solution and its pH is crucial for the electro-oxidation of organic compounds. The pH of the supporting electrolyte plays a significant role in electrochemical reactions, since protons are involved in them, affecting both i_p and E . To investigate the supporting electrolyte effect, a 0.1 M ABS was tested at different pH values. The pH effect (from 3.17 to 6.56) on the electrode reaction was studied using CV (Fig. S4). As shown in Fig. S4b, anodic i_p increased with increasing pH, up to 4.5, and then decreased. Therefore, all measurements in this study were conducted at a pH of 4.5. The relationship between E_p and pH was also examined. Anodic E_p shifted towards less positive E values, with an increase in pH, indicating direct involvement of protons in the oxidation process. E_{pa} - pH plot (Fig. S4c) showed that the dependence of E_{pa} on pH could be described by the following equation:

$$E_{pa} = -81.85 \text{ mV} \cdot \text{pH} + 1439 \quad (R^2 = 0.976) \quad (2)$$

The slope of -81.85 mV/pH indicates that the number of protons involved in the process was equal to the number of transferred electrons.

SR effect

In electrochemical studies, useful information, such as electrochemical reaction mechanism and kinetic parameters, usually can be found from E^0 of SR. Therefore, SR effect on SFA (1×10^{-4} M) electrochemical behavior was investigated (Fig. 5a). Recorded CV revealed that i_p increased by increasing SR from 0.02 to 0.16 V/s. A linear relationship was obtained by plotting anodic i_p vs. SR root (Fig. 5b). The corresponding equation can be expressed as:

$$I_{pa} (\mu\text{A}) = 72.66v^{1/2} (\text{V/s})^{1/2} + 0.893 \quad (R^2 = 0.979) \quad (3)$$

As shown in Fig. 5c, a linear relationship was also obtained for logarithmic i_p vs. logarithmic SR, which can be expressed as:

$$\log I_{pa} (\mu\text{A}) = 0.454 \log v (\text{V/s}) + 1.823 \quad (R^2 = 0.979) \quad (4)$$

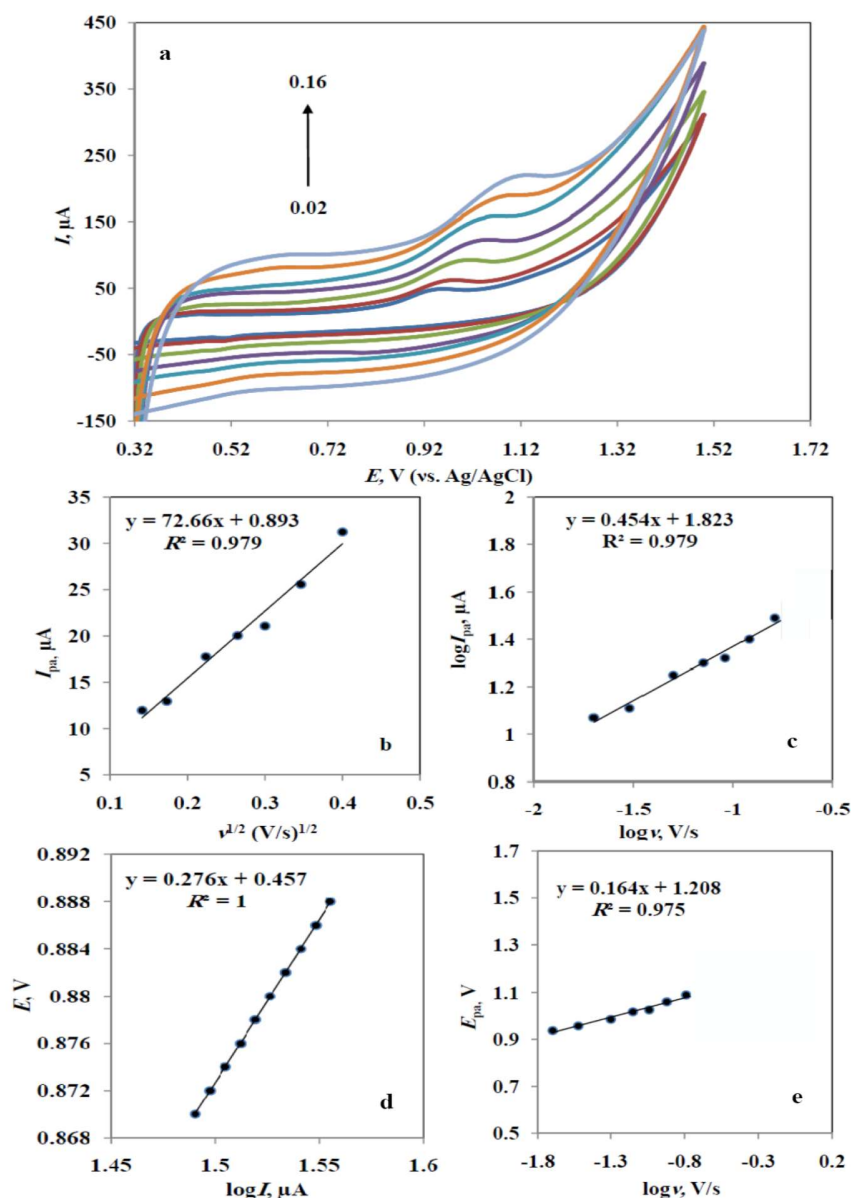


Figure 5: (a) CV for 10^{-4} M SFA on HNS from CuO/ZnO/MWCNT/GCE, at different SR, from 0.02 to 0.16 V/s; (b) plot of anodic i_p vs. SR root; (c) plot of logarithmic i_p vs. logarithmic SR; (d) Tafel plot; and (e) dependence of E_p and logarithmic SR ($\log v$).

Its slope (0.454) was close to the theoretical value of 0.5. These results indicate that SFA's oxidation on HNS from CuO/ZnO/MWCNT/GCE was a diffusion-controlled process [44]. Moreover, as SR increased, E_p shifted to higher positive E , which confirmed the oxidation process irreversibility. To obtain information on the rate-determining step, Tafel plot was drawn using the rising part of I-V curve for SFA monitored at a SR of 0.05 V/s (Fig. 5d). This part of the CV known as Tafel region was affected by electron transfer kinetics between SFA and HNS from CuO/ZnO/MWCNT/GCE. The slope of this plot was 0.276 V/decade, indicating that

$\alpha = 0.78$. The dependence of E_p and logarithmic SR ($\log v$) showed a linear relationship with a regression equation of E_{pa} (V) = 0.164 $\ln v$ (V/s) + 1.208 ($R^2 = 0.975$) (Fig. 5e). For an irreversible electrode process, according to Laviron's equation [45], E_{pa} is defined by the following expression:

$$E_{pa} = E^{o'} + \frac{RT}{(1-\alpha)nF} \ln \frac{(1-\alpha)nF}{RT s} + \frac{RT}{(1-\alpha)nF} \ln v \quad (5)$$

where $T = 298.15$ K, $F = 96485$ mol⁻¹ and $R = 8.314$ J/molK). Further, n involved during SFA oxidation in an ABS, at HNS from CuO/ZnO/MWCNT/GCE, was calculated as $0.81 \approx 1$. Also, if $E^{o'}$ value is known, k_s value can be determined from the intercept of E_p straight line vs. $\log v$ (Eq. 5). $E^{o'}$ in Eq. (5) was obtained from the intercept of E_p vs. v curve, by extrapolating to the vertical axis, at $v = 0$. From intercept (1.208 V) and $E^{o'}$ (0.9286), k_s value was calculated as 4.5×10^{-3} s⁻¹.

Chronoamperometric study of SFA

The chronoamperometric study was employed to evaluate the D_0 of SFA. Fig. 5a shows chronoamperograms obtained using HNS from CuO/ZnO/MWCNT/GCE in SFA's presence. D_0 for SFA was determined using Eq. (6):

$$I = nFAC(D/\pi t)^{1/2} \quad (6)$$

From the slope of a plot of slopes of Cottrell plots vs. Ct of SFA (Fig. 5b), corresponding to equation $y = 11.58x + 62.37$; $R^2 = 0.994$, D_0 value of SFA was estimated to be 2.84×10^{-6} cm²/s.

Calibration curve

In order to test the feasibility of this method for SFA quantitative analysis, the relationship between its Ct and anodic i_p was studied using DPV (Fig. 6a).

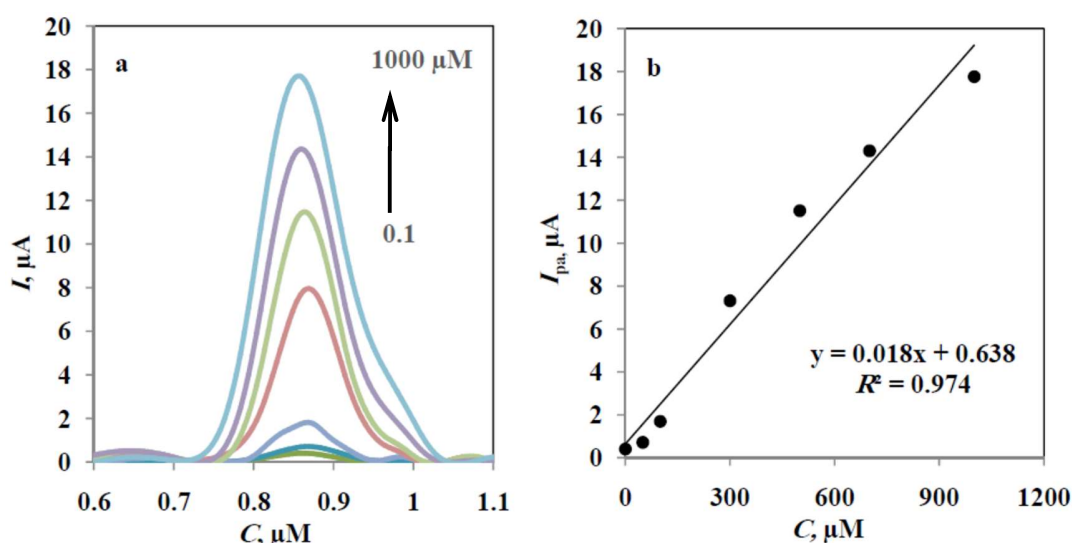


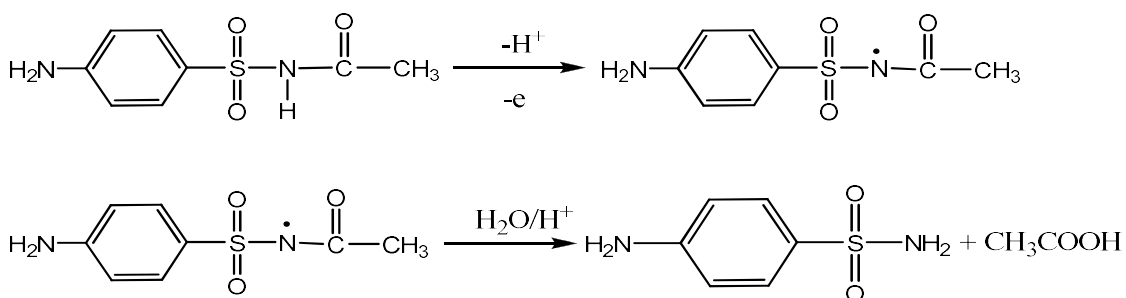
Figure 6: (a) Plot of DPV anodic i_p and Ct of SFA; (b) calibration curve.

Under optimized conditions, the calibration curve (Fig. 6b) was linear, in the range from 0.1 to 1000 μM . The regression equation was:

$$I_{pa}(\mu\text{A}) = 0.018C + 0.638 \quad (R^2 = 0.974) \quad (7)$$

LoD (S/N = 3) and LoQ (S/N = 10) were 0.089 and 0.297 μM , respectively.

To estimate the repeatability of the proposed electrode, RSD from three successful i_p measurements of a 1×10^{-4} M SFA solution, at HNS from CuO/ZnO/MWCNT/GCE, was calculated to be 1.96%, demonstrating the good repeatability of the proposed electrode. The reproducibility and stability of the proposed electrode were also explored. The reproducibility RSD between electrodes was investigated using three similar HNS from CuO/ZnO/MWCNT/GCE electrodes in a 1×10^{-4} M SFA solution. RSD was 3.36%, which demonstrated excellent reproducibility. The stability of the modified electrode was also observed to be good. As mentioned in the previous section, n in the electrode reaction was 1. The possible reaction pathway for the electro-oxidation of SFA on HNS from CuO/ZnO/MWCNT/GCE in a 0.1 M ABS (pH = 4.5) is proposed in Scheme 1.



Scheme 1: SFA's proposed oxidation reaction.

SFA oxidation ensued at the NH group of the amide moiety, producing a thermodynamically unstable radical in different isomeric states. The radical's stabilization occurred through water nucleophilic addition to the acetyl group, resulting in a $-\text{SO}_2\text{NH}_2$ moiety and CH_3COOH .

Interference effect

It is widely acknowledged that certain electroactive species and structurally related drugs may affect sensors' performance. Therefore, the selectivity of the proposed electrode towards SFA was investigated by introducing foreign species, such as UA, AA, Glu, various ions (Mg^{2+} , K^+ , Na^+ , Cu^{2+} and Ca^{2+}) and some formulation ingredients of SFA, including BNZ, EDTA and PA. The impact of these interference substances was evaluated in the presence of 4×10^{-4} M SFA, in an ABS at pH = 4.5, by measuring the changes in anodic i_p , before and after the addition of different foreign interferences. The tolerance limit was defined as the maximum Ct of the interfering substance, which gave an error in the range of $\pm 10\%$ in SFA determination (Table 1).

Table 1: Tolerance of interferences on SFA determination.

Interference substances	Tolerance level ratio
Mg ²⁺ , K ⁺ , Na ⁺ , Cu ²⁺ and Ca ²⁺	110
Glu	130
AA	300
UA	85
EDTA	190
BNZ	0,8
PA	0,1

The results obtained with amperometry and DPV demonstrated high selectivity of HNS from CuO/ZnO/MWCNT/GCE, for SFA detection (Fig. 7).

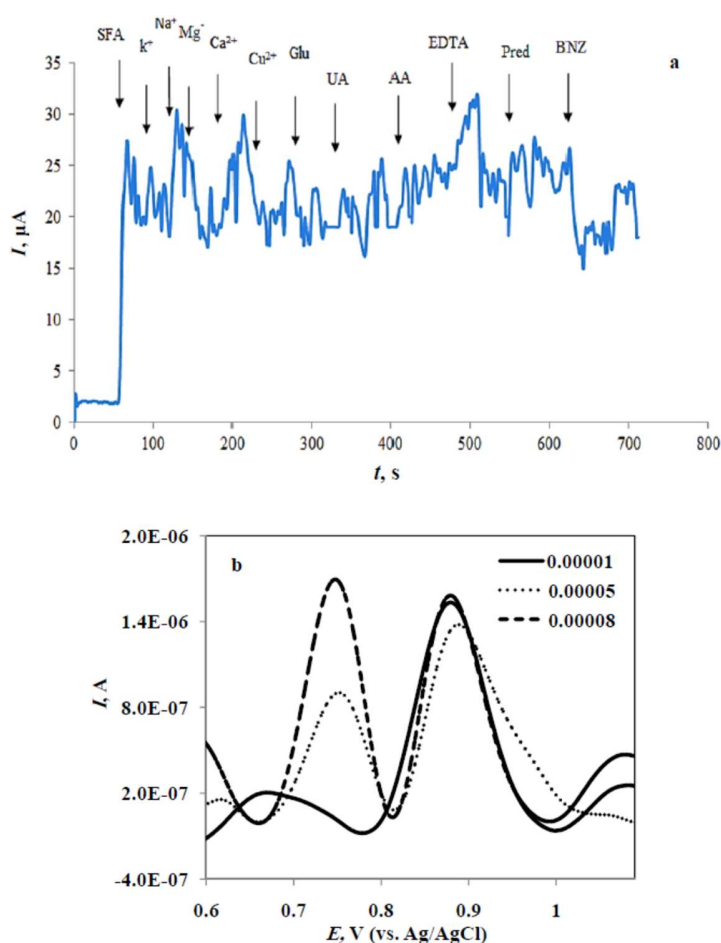


Figure 7: (a) Interference effect of foreign substances on electrochemical response of HNS from CuO/ZnO/MWCNT/GCE in a 4×10^{-4} M SFA solution (pH=4.5); (b) Plot of DPV from SFA in different Ct of BNZ (1×10^{-5} , 5×10^{-5} and 8×10^{-5} M) in an ABS (pH = 4.5), at a SR of 0.1 V/s.

Application

To assess the efficacy of the proposed electrode, SFA identification and quantification in blood serum, SFA sodium 10% eye drop and WW samples were directly analyzed

using the standard addition method and DPV technique. Under optimal conditions, representative DPVs for eye drop and serum samples are depicted in Fig. 8. The observed oxidation peak of SFA increased upon adding its standard solutions to both samples. The obtained results for SFA sodium 10% eye drop and serum samples, before and after spiking, are shown in Table 2. Industrial WW samples with SFA were studied using DPV and UV-vis spectrophotometric methods. The calibration curve was drawn using standard solutions, to evaluate SFA's maximum wavelength, which was 269 nm. All calculations were performed at this wavelength. Fig. S6 shows UV-vis plot and DPV of SFA in the WW sample with an ABS. Evaluation of these results indicates that the values obtained by CV (13.44 ± 0.13 mM; %RSD = 0.97 (n = 3)) were in good agreement with those acquired by the spectrophotometric method (13.37 ± 0.08 mM; %RSD = 0.59 (n = 3)). Statistical calculations indicate good agreement between mean values (t-test, 0.34) and precision (F-test, 2.64), for the two methods (P = 0.05).

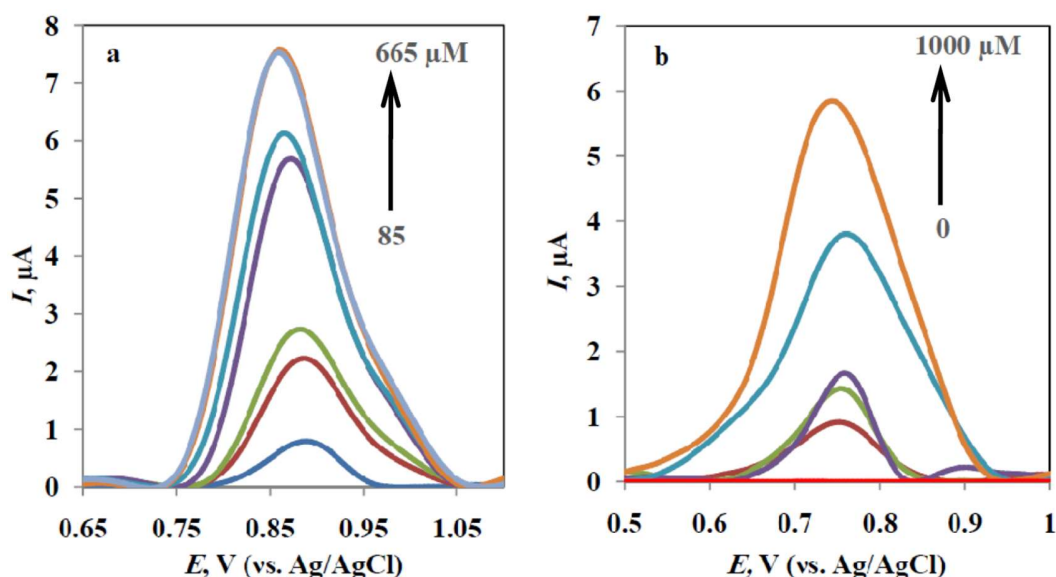


Figure 8: Plot of DPV of SFA in ABS (pH=4.5) containing (a) SFA sodium eye drop and (b) blood serum.

13

Table 2: Determination results for SFA in SFA sodium 10% drop and blood serum.

Sample	Added SFA (μM)	Calculated SFA (μM)	Recovery (%)	RSD (%)
SFA sodium 10% drop	423	424 ± 6	100.21	1.4
	100	99.5 ± 1.2	99.5	1.2
Blood serum	500	484 ± 8.5	96.8	1.8
	1000	988 ± 12.4	98.8	1.3

Table 3 summarizes the characteristics of sensors reported in the literature for SFA determination.

Table 3: Characteristics of the sensors for SFA determination in model solutions, drugs, and physiological media.

Modifier	Sample	Method	Linear range/LoD (M)	pH	Ref
PFSA membranes + CNT	Sulfacyl sodium (Albucid)	Potentiometry	10-4- 10-2/1.72 × 10-7	5-8	[36]
Pyrolytic graphite sensor covered by embedded poly 1,5-diaminonaphthalene CNT	Locula 20 and 30% Albucid (eye drops)	SWV	5 × 10-6- 1.5 × 10-3/ 1.1 × 10-7	7.2	[30]
CPE	Model solution	SWV	10-6- 10-3/4 × 10-7	6.0	[46]
PVC matrix + tetradodecylammonium bromide + 2-nitrophenyl octyl ether	Model solution, Rabbit aqueous humor, Blephamide® (ophthalmic suspension), Ocusol® 10 and 20% (eye drops)	Potentiometry	10-4.5- 10-2/ 2.23 × 10-5	5-7	[47]
PVC matrix + sulphadiazine + cetyltriocetylammmonium complex+ cholestyramine	Model solution	PQCR	8 × 10-7- 5 × 10-5/ 5 × 10-7	8.63	[48]
Cu(I) complexes at HMDE	Model solution	CSV	10-8- 1.5 × 10-7/10-9	6	[49]
HNS from CuO/ZnO/MWCNT	Blood serum, SFA sodium 10% eye dro and WW	DPV	10-7- 10-3/ 8.9 × 10-8	4.5	This work

Each method has its distinct advantages and features. Data for Ct, LoD and accuracy of SFA determination, using the developed technique and methods described in Table 3, are similar. In addition, the developed sensor shows significantly longer stability, which is crucial for practical applications. The established method is straightforward, reagent-free, and requires no sample preparation.

Conclusions

In this study, a new, cost-effective and time-saving method was introduced to synthesize HNS from CuO/ZnO, using complex-directed hybridization and subsequent calcination techniques. The synthesized HNS from CuO/ZnO were combined with MWCNT, to form a novel NC that was employed to modify the GCE. SFA's electrochemical behavior was investigated on the HNS from CuO/ZnO/MWCNT/GCE, in an ABS of pH 4.5. Compared to the HNS from CuO/ZnO/MWCNT/GCE and GCE, SFA's anodic i_p was the highest, and the E_p was the lowest at the HNS from CuO/ZnO/MWCNT/GCE. The combination of HNS from CuO/ZnO with MWCNT produced a synergistic effect, due to their unique properties. Under optimized conditions, anodic i_p was linearly proportional to Ct of SFA, over a wide linear range (10^{-7} to 10^{-3} M), and LoD was approximately 0.089 μ M. The obtained results were promising, and show the potential of the proposed method, for determining the Ct of SFA in biological fluids, without requiring complex sample pretreatment.

Acknowledgements

The authors express their gratitude to the post-graduate office of Guilan University, for providing support for this study.

Authors' contributions

Majid Arvand: supervision; methodology; validation; reviewing and editing. **Talat P.-Saravani:** data curation; writing; original draft preparation. **Farhang Mizani:** software; methodology; validation. **Akram Pourhabib:** software; methodology; validation; original draft preparation.

Abbreviations

AA: ascorbic acid

ABS: acetate buffer solution

Ag/AgCl: silver/silver chloride

BNZ: benzalkonium chloride

C: carbon

CH₃COOH: acetic acid

CH₃COONa: sodium acetate

CNT: carbon nanotube

CSV: cathodic stripping voltammetry

Ct: concentration

Cu(NO₃)₂: copper nitrate

CuO: copper oxide

CV: cyclic voltammetry

DMF: dimethylformamide

DPV: differential pulse voltammetry

EDTA: disodium ethylenediaminetetraacetic acid salt

EDX: energy dispersive X-ray analysis

[Fe(CN)₆]^{3-/4-}: ferrocyanide

FT-IR: Fourier transform infrared spectroscopy

GCE: glassy carbon electrode

Glu: glucose

H₂C₂O₄·2H₂O: oxalic acid

HCl: hydrogen chloride

HMDE: hanging mercury drop electrode

HNS: hybrid nanostructure

K₃[Fe(CN)₆]: potassium hexacyanoferrate(III)

K₄[Fe(CN)₆]: potassium ferrocyanide

KCl: potassium chloride

LoD: limit of detection

LoQ: limit of quantification

MWCNT: multi-walled carbon nanotube

Na: sodium

NC: nanocomposite

NiO: nickel oxide

NP: nanoparticles

PA: prednisolone acetate

PFSA: perfluorosulfonic acid

PQCR: piezoelectric quartz crystal resonator

Pt: platinum

Redox: reduction/oxidation reactions

RSD: relative standard deviation
Sc: semiconductor
SEM: scanning electron microscopy
SFA: sodium sulfacetamide
SnO₂: tin(IV) oxide
SR: scan rate (v)
SWV: square wave voltammetry
TEM: transmission electron microscopy
TiO₂: titanium oxide
UA: uric acid
UV-vis: visible ultra-violet light
Zn(CH₃CO₂)₂: zinc acetate
ZnO: zinc oxide
WW: wastewater

Symbols

α : transfer coefficient
A: effective surface area
D₀: diffusion coefficient
E^o: formal potential
E_{gap}: bandgap energy
E_p: peak potential
E_{pa}: oxidation potential
i_p: peak current
k_s: rate constant of an electrochemical reaction
 μm : micrometer
n: number of electrons transferred
nm: nanometer
n-type: semiconductor with an added pentavalent impurity
p-type: semiconductor with an added trivalent impurity
R²: coefficient of determination

References

1. Das S, Srivastava VC. An overview of the synthesis of CuO-ZnO nanocomposite for environmental and other applications. *Nanotechnol Rev.* 2018;7:267-82. <https://doi.org/10.1515/ntrev-2017-0144>
2. Saravanan R, Karthikeyan S, Gupta VK et al. Enhanced photocatalytic activity of ZnO/CuO nanocomposite for the degradation of textile dye on visible light illumination. *Mater Sci Eng C.* 2013;33:91-98. <https://doi.org/10.1016/j.msec.2012.08.011>

- Bandara J, Pradeep UW, Bandara RGST. The role of n-p junction electrodes in minimizing the charge recombination and enhancement of photocurrent and photovoltage in dye sensitized solar cells. *J Photochem Photobiol A Chem.* 2005;170:273-78. <https://doi.org/10.1016/j.jphotochem.2004.08.023>
- Anicai L, Petica A, Patroi D et al. Electrochemical synthesis of nanosized TiO₂ nanopowder involving choline chloride based ionic liquids. *Mater Sci Eng B.* 2015;199:87-95. <https://doi.org/10.1016/j.mseb.2015.05.005>
- Mariammal RN, Ramachandran K, Renganathan B et al. On the enhancement of ethanol sensing by CuO modified SnO₂ nanoparticles using fiber-optic sensor. *Sens Actuat B.* 2012;169:199-207. <https://doi.org/10.1016/j.snb.2012.04.067>
- Yang H, Tao Q, Zhang X et al. Solid-state synthesis and electrochemical property of SnO₂/NiO nanomaterials. *J Alloy Compd.* 2008;459:98-102. <https://doi.org/10.1016/j.jallcom.2007.04.258>
- Suvith VS, Devu VS, Philip D. Facile synthesis of SnO₂/NiO nano-composites: Structural, magnetic and catalytic properties. *Ceram Int.* 2020;46:786-794. <https://doi.org/10.1016/j.ceramint.2019.09.033>
- Jin Z, Zhang X, Li Y et al. 5.1% apparent quantum efficiency for stable hydrogen generation over eosin-sensitized CuO/TiO₂ photocatalyst under visible light irradiation. *Catal Commun.* 2007;8:1267-73. <https://doi.org/10.1016/j.catcom.2006.11.019>
- Li B, Hao Y, Zhang B et al. A multifunctional noble-metal-free catalyst of CuO/TiO₂ hybrid nanofibers. *Appl Catal A: Gen.* 2017;531:1-12. <https://doi.org/10.1016/j.apcata.2016.12.002>
- Jun ST, Choi GM. Composition dependence of the electrical conductivity of ZnO(n)-CuO(p) ceramic composite. *J Am Ceram Soc.* 1998;81:695-99. <https://doi.org/10.1111/j.1151-2916.1998.tb02391.x>
- Zhang D. Synthesis and characterization of ZnO-doped cupric oxides and evaluation of their photocatalytic performance under visible light. *Transit Met Chem.* 2010;35:689-94. <https://doi.org/10.1007/s11243-010-9380-z>
- Wang RC, Lin HY. ZnO-CuO core-shell nanorods and CuO-nanoparticle-ZnO-nanorod integrated structures. *Appl Phys A.* 2009;95:813-818. <https://doi.org/10.1007/s00339-009-5079-4>
- Zaoui A, Ferhat M, Ahuja R. Magnetic properties of (ZnO)₁/(CuO)₁(001) superlattice. *Appl Phys Lett.* 2009;94:102102. <https://doi.org/10.1063/1.3095811>
- Gajendiran J, Rajendran V. Synthesis and characterization of coupled semiconductor metal oxide (ZnO/CuO) nanocomposite. *Mater Lett.* 2014;116:311-13. <https://doi.org/10.1016/j.matlet.2013.11.063>
- Nakamura Y, Yoshioka N, Miyayama M et al. Selective CO gas sensing mechanism with CuO / ZnO heterocontact. *J Electrochem Soc.* 1990;137:940-43. <https://doi.org/10.1149/1.2086583>

16. Ushio Y, Miyayama M, Yanagida H. Effects of interface states on gas-sensing properties of a CuO/ZnO thin-film heterojunction. *Sens Actuat B*. 1994;17:221-26. [https://doi.org/10.1016/0925-4005\(93\)00878-3](https://doi.org/10.1016/0925-4005(93)00878-3)
17. Baek KK, Tuller HL. Atmosphere sensitive CuO/ZnO junctions. *Solid State Ionics*. 1995;75:179-86. [https://doi.org/10.1016/0167-2738\(94\)00172-O](https://doi.org/10.1016/0167-2738(94)00172-O)
18. Li B, Wang Y. Facile synthesis and photocatalytic activity of ZnO–CuO nanocomposite. *Superlat Microstruct*. 2010;47:615-23. <https://doi.org/10.1016/j.spmi.2010.02.005>
19. Simon Q, Barreca D, Gasparotto A et al. Vertically oriented CuO/ZnO nanorod arrays: from plasma-assisted synthesis to photocatalytic H₂ production. *J Mater Chem*. 2012;22:11739-747. <https://doi.org/10.1039/C2JM31589K>
20. Vijayakumar GNS, Devashanka S, Rathnakumari M et al. Synthesis of electrospun ZnO/CuO nanocomposite fibers and their dielectric and non-linear optic studies. *J Alloys Compd*. 2010;507:225-29. <https://doi.org/10.1016/j.jallcom.2010.07.161>
21. Sathishkumar P, Sweena R, Wu JJ et al. Synthesis of CuO-ZnO nanophotocatalyst for visible light assisted degradation of a textile dye in aqueous solution. *Chem Eng J*. 2011;171:136-40. <https://doi.org/10.1016/j.cej.2011.03.074>
22. Yang C, Cao X, Wang S et al. Complex directed hybridization of CuO/ZnO nanostructures and their gas sensing and photocatalytic properties. *Ceram Int*. 2015;41:1749-56. <https://doi.org/10.1016/j.ceramint.2014.09.120>
23. Harisha S, Archana J, Sabarinathana M et al. Controlled structural and compositional characteristic of visible light active ZnO/CuO photocatalyst for the degradation of organic pollutant. *Appl Surf Sci*. 2017;418:103-12. <https://doi.org/10.1016/j.apsusc.2016.12.082>
24. Zhao M, Wang X, Ning L et al. Electrospun Cu-doped ZnO nanofibers for H₂S sensing. *Sens Actuat B*. 2011;156:588-92. <https://doi.org/10.1016/j.snb.2011.01.070>
25. Wang JX, Sun XW, Yang Y et al. Free-standing ZnO–CuO composite nanowire array films and their gas sensing properties. *Nanotechnology*. 2011;22:325704. <https://doi.org/10.1088/0957-4484/22/32/325704>
26. Karunakaran C, Manikandan G. Synthesis and characterization of Zn-doped CuO nanomaterials for electrochemical supercapacitor applications. *Rec Adv Surf Sci*. 2013:93-95. ISBN 978-93-82338-36-9
27. Yang J, Jiang LC, Zhang WD et al. A highly sensitive non-enzymatic glucose sensor based on a simple two-step electrodeposition of cupric oxide (CuO) nanoparticles onto multi-walled carbon nanotube arrays. *Talanta*. 2010;82:25-33. <https://doi.org/10.1016/j.talanta.2010.03.047>
28. Kang X, Mai Z, Zou X et al. A sensitive nonenzymatic glucose sensor in alkaline media with a copper nanocluster/multiwall carbon nanotube-modified glassy carbon electrode. *J Analyt Biochem*. 2007;363:143-50. <https://doi.org/10.1016/j.ab.2007.01.003>

29. Fuchs SM, Elsner P. Sulfonamides in dermatology. *Clin Dermatol.* 2003;21:7-11. [https://doi.org/10.1016/s0738-081x\(02\)00326-7](https://doi.org/10.1016/s0738-081x(02)00326-7)
30. Yadav SK, Choubey PK, Agrawal B et al. Carbon nanotube embedded poly 1,5-diaminonaphthalene modified pyrolytic graphite sensor for the determination of sulfacetamide in pharmaceutical formulations. *Talanta.* 2014;118:96-103. <https://doi.org/10.1016/j.talanta.2013.09.061>
31. Raviolo MA, Rambla-Alegre M, Clausell-Tormos J et al. Determination of sulfonamides in milk after precolumn derivatisation by micellar liquid chromatography. *J Analyt Chim Acta.* 2007;593:152-56. <https://doi.org/10.1016/j.aca.2007.05.001>
32. Posyniak A, Zmudzki J, Mitrowska K. Dispersive solid-phase extraction for the determination of sulfonamides in chicken muscle by liquid chromatography. *J Chromat A.* 2005;1087:259-64. <https://doi.org/10.1016/j.chroma.2005.01.044>
33. Errayess SA, Lahcen AA, Idrissi L et al. A sensitive method for the determination of sulfonamides in seawater samples by solid phase extraction and UV-Visible spectrophotometry. *Spectrochim Acta Part A: Mol Biomol Spectrosc.* 2017;181:276-85. <https://doi.org/10.1016/j.saa.2017.03.061>
34. Fuh MRS, Chu SY. Quantitative determination of sulfonamide in meat by solid-phase extraction and capillary electrophoresis. *Analyt Chim Acta.* 2003;499:215-21. [https://doi.org/10.1016/S0003-2670\(03\)00721-9](https://doi.org/10.1016/S0003-2670(03)00721-9)
35. Ahmed S, Anwar N, Sheraz MA et al. Validation of a stability-indicating spectrometric method for the determination of sulfacetamide sodium in pure form and ophthalmic preparations. *J Pharm Bioallied Sci.* 2017;9:126-34. <https://doi.org/10.4103/jpbs.JPBS-184-16>
36. Safronova E, Parshina A, Kolganova T et al. Potentiometric multisensory system based on perfluorosulfonic acid membranes and carbon nanotubes for sulfacetamide determination in pharmaceuticals. *J Electroanal Chem.* 2020;873:114435. <https://doi.org/10.1016/j.jelechem.2020.114435>
37. Balakrishnan VK, Terry KA, Toito J. Determination of sulfonamide antibiotics in wastewater: A comparison of solid phase microextraction and solid phase extraction methods. *J Chromat A.* 2006;1131:1-10. <https://doi.org/10.1016/j.chroma.2006.07.011>
38. Viswanatha R, Venkatesh TG, Vidyasagar CC et al. Preparation and characterization of ZnO and Mg-ZnO nanoparticle. *Arch Appl Sci Res.* 2012;4:480-86.
39. Dubal DP, Gund GS, Holze R et al. Surfactant-assisted morphological tuning of hierarchical CuO thin films for electrochemical supercapacitors. *Dalton Trans.* 2013;42:6459-67. <https://doi.org/10.1039/C3DT50275A>
40. Jafari A, Ghane M, Sarabi M et al. Synthesis and antibacterial properties of zinc oxide combined with copper oxide nanocrystals. *Orient J Chem.* 2011;27:811-22.
41. Shinde SK, Dubal DP, Ghodake GS et al. Influence of Mn incorporation on the supercapacitive properties of hybrid CuO/Cu(OH)₂ electrodes. *RSC Adv.* 2015;5:30478-484. <https://doi.org/10.1039/C5RA01093D>

42. Bard AJ, Faulkner LR. *Electrochemical Methods: Fundamentals and Applications*. 2nd ed., John Wiley & Sons, New York, 2004.
43. Zoski CG. *Handbook of Electrochemistry*. 1st ed., Elsevier Science, Amsterdam, 2007.
44. Gosser DK. *Cyclic Voltammetry: Simulation and Analysis of Reaction Mechanisms*. VCH, New York, 1993.
45. Laviron E. General expression of the linear potential sweep voltammogram in the case of diffusionless electrochemical systems. *J Electroanal Chem Interfac Electrochem*. 1974;101:19-28. [https://doi.org/10.1016/S0022-0728\(79\)80075-3](https://doi.org/10.1016/S0022-0728(79)80075-3)
46. Ait Lahcen A, Ait Errayess S, Amine A. Voltammetric determination of sulfonamides using paste electrodes based on various carbon nanomaterials. *Microchim Acta*. 2016;183:2169-76. <https://doi.org/10.1007/s00604-016-1850-3>
47. El-Ragehy NA, Hegazy MA, Abd El HG et al. Validated potentiometric method for the determination of sulfacetamide sodium; application to its pharmaceutical formulations and spiked rabbit aqueous humor. *Bull Fac Pharm Cairo Univ*. 2018;56:207-12. <https://doi.org/10.1016/j.bfopcu.2018.08.002>
48. Yuan J, Yao S. A sulpha-drug sensitive sensor based on ion-pair complex modified PQC resonator. *Talanta*. 2002;58:641-48. [https://doi.org/10.1016/S0039-9140\(02\)00309-0](https://doi.org/10.1016/S0039-9140(02)00309-0)
49. Fogg AG, Yusoff ARHM, Moreira JC et al. Cathodic stripping voltammetric determination of sulfonamides as copper(I) complexes at a hanging mercury drop electrode. *Analyt Proc*. 1995;32:95-97. <https://doi.org/10.1039/AI9953200095>